DOI 10.1007/s11595-016-1498-1

Effect of Thermal Shock Process in Accelerated Environment Spectrum on the Fatigue Life of 7B04-T6 Aluminum Alloy

CUI Tengfei, LIU Daoxin, ZHANG Xiaohua, YU Shouming
(Institute of Corrosion and Protection, Northwestern Polytechnical University, Xi'an 710072, China)

Abstract: The effect of thermal shock, in an accelerated-corrosion environment spectrum, on the fatigue and corrosion behavior of 7B04-T6 aluminum alloy, was determined. The environment spectrum consists of two modules, namely: salt-spray corrosion and thermal shock. The effect of thermal shock on the mechanical properties was determined via tensile tests; SEM, DCS, and XRD were used to determine the effect of thermal shock on the corrosion products. In addition, the corrosion resistance of the products was ascertained through electrochemical testing. The results show that the mechanical properties and fatigue life of the aluminum alloy will decline with prolonged thermal shock time. The thermal shock process may result in denser surface corrosion products than those formed on the no thermal shock specimens, and transformation of some $Al(OH)_3$ into AlOOH. AlOOH may have resulted in improved corrosion resistance and hence a lower decrease in the fatigue life after corrosion, compared with that of the no thermal shock specimen. Repeated corrosion/thermal shock may have delayed further decease in the fatigue life. Therefore, selection of an appropriate equivalent thermal shock temperature and time was essential for designing the environmental spectrum.

Key words: accelerated corrosion environment spectrum; thermal shock; corrosion; fatigue; aluminum alloy

1 Introduction

The Lord/environment spectrum is the main technique used to forecast the service life of aircraft structures. In fact, designing this spectrum constitutes an important task in the fatigue/durability/damage tolerance design of these structures. Compiling a suitable spectrum that simulates the actual conditions of the structure is essential for ensuring aircraft safety and reducing the costs associated with aircraft fabrication[1,2]. Military aircraft typically (*i e*, more than 95% of the service time) are parked at the airport and less than 5% of the time is spent on duty or training in the air. During parking, damage to the aircraft structure results primarily from environmental corrosion. This is especially true in the case of coastal areas, where corrosion damage is more severe than in non-coastal regions[3-5]. During flight, however, the aircraft structure undergoes mainly fatigue loading and the content of humidity/erosive ions is low; hence, during flight, the aircraft suffers mainly fatigue damage[6-8]. Damage to the structure can therefore be described as "corrosion in the airport + fatigue in the air".

With the development of aerospace technologies, modern military aircraft operate at high flying speed and exhibit good maneuverability. During the takeoff or landing and high-speed maneuvering, however, the friction between the structure and the atmosphere results in an increase in the temperature. This increase may have an adverse effect on the aircraft structure[9,10]. Therefore, the selection of a suitable equivalent thermal shock temperature and thermal shock time is critical to the design of the environment spectrum. Currently, the aircraft load/environment spectrum used in China is based on the accelerated test load/environment spectrum (applicable to subtropical coastal areas and structures covered by a coating-CASS) - CASS was designed by the United States Air Force. The environment spectrum in CASS is described as "corrosion + thermal shock". In CASS, 1 h of thermal shock at 149 ℃ is equivalent to a one-year increase in the temperature of the component. Aluminum alloy

(Received: Oct. 18, 2015; Accepted: July 7, 2016)
CUI Tengfei(崔腾飞): Ph D; E-mail: 33076873@qq.com
*Corresponding author: LIU Daoxin(刘道新): Prof.; Ph D.; E-mail: Liudaox@nwpu.edu.cn

structures are widely used in present-day aircraft in order to reduce the weight of the aircraft. However, owing to its low aging temperature, the alloy undergoes artificial aging at 149 ℃[11-14]; Corrosion products are also sensitive to temperature changes. Our previous research has shown that using CASS as a reference may lead to a laboratory life that is significantly longer than the actual life. This large deviation stems mainly from the temperature increase resulting from thermal shock. The mechanisms governing a combined thermal shock-corrosion process must therefore be determined.

As such, in this work, the effect of the thermal shock process on the fatigue life of aluminum alloys was determined; This study was performed on the 7B04-T6 aircraft aluminum alloy. The results obtained can be used to provide the basis for designing a scientific and rational environment spectrum of aircraft structures.

2 Experimental

2.1 Materials

A standard commercial 7B04-T6 aluminum alloy (AA7B04) was investigated in this work. The alloy was 3 mm-thick, and had a chemical composition (wt%) of: 6.0% Zn, 2.5% Mg, 1.5% Cu, 0.15% Fe, 0.5% Mn, 0.1% Si, 0.05% Ti, Al balance. This alloy had the following mechanical properties: yield strength (YS)=537 MPa, ultimate tensile strength (UTS)=596 MPa, and final shrinkage=32%. Prior to the tests, the specimens were all polished using alumina paper ranging from 240# to 1000#, degreased with acetone, rinsed with deionized water, and dried with clean compressed air. Fig.1 shows a schematic of the specimen geometry.

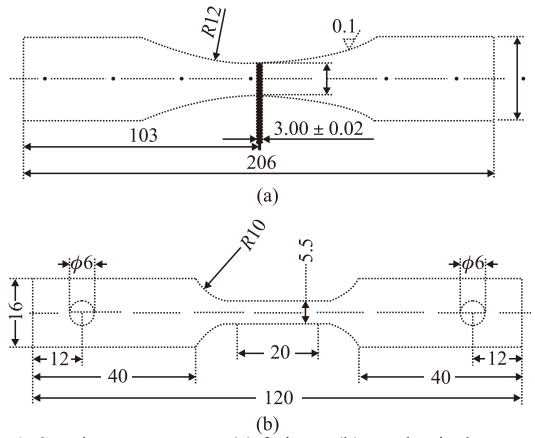

Fig.1 Specimen geometry: (a) fatigue; (b) mechanical property

The climate data of a certain city in the north of China (whose climatic features can be described as an industrial-oceanic climate) were collected. CASS was consulted, and then we designed the accelerated environment spectrum of this city. The equivalent environment spectrum was salt-spray corrosion, and the solution concentration, pH value, and temperature were 5 wt% NaCl, 4 (dilute-sulfuric-acid-adjusted pH), and 40 ℃, respectively. Furthermore, 90 h of salt-spray corrosion in the laboratory is equivalent to 1 year of corrosion in the aforementioned city. After this corrosion, the specimens were subjected to 1 h of thermal shock at 149 °C; This shock treatment is equivalent to a 1-year temperature change during the process of takeoffs or landings and high-speed maneuvering in the air. The specimens were also subjected to constant-amplitude fatigue tests, where σ_{max}=180 MPa and R=0.06.

2.2 Effect of thermal shock process on the fatigue life

To determine the effect of the thermal shock time on the fatigue life of AA7B04, the following tests were performed: thermal shock (TS) for various times (no TS, 2, 4, 6, 8, and 10 h), corrosion for 90 h, and then fatigue tests; the details of these tests are shown in Fig.2 (a).

To determine the effect of the TS time on the corrosion products, the following tests were performed: 90 h of corrosion, TS for various times (no TS, 2, 6, and 10 h), another 90 h of corrosion, and then fatigue tests; the details of these tests are shown in Fig.2 (b).

To determine the effect of the number of TS cycles on the fatigue life, samples were subjected to corrosion and TS for 180 and 10 h, respectively (as shown in Fig.2 (c)).

Electrochemical impedance spectroscopy (EIS) was performed and Mott-Schottky curves were obtained by using a PARSTAT-2273. Three electrode systems were utilized; working electrode: aluminum alloy, auxiliary electrode: platinum sheet, and reference electrode: saturated calomel electrode. EIS scans were performed over a frequency range and at an excitation voltage of 10^{-2}-10^{5} Hz and 10 mV, respectively. Moreover, Mott–Schottky curves were obtained over a scan voltage range of −0.9 to −0.5 V and at a frequency of 10^{4} Hz.

We used a Mettler-Toledo thermal analysis instrument to analyze the transformation of $Al(OH)_3$, at a heating rate of 10 ℃/min during the TS process. In addition, we used XRD to analyze the transformation

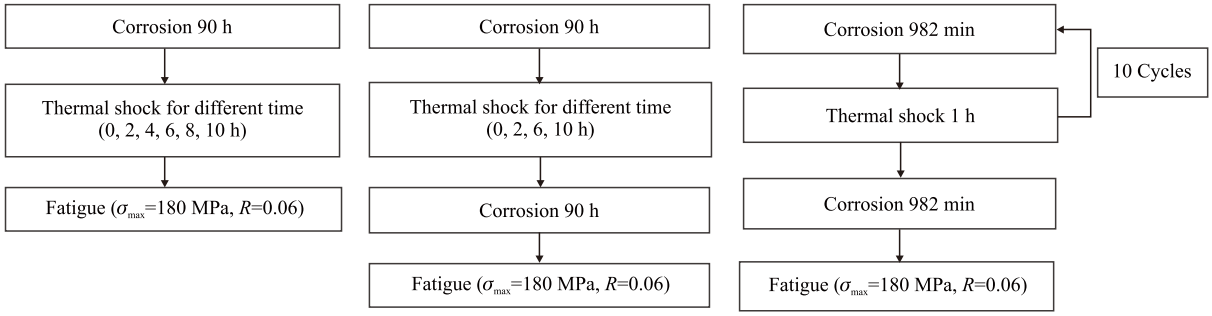

Fig.2 Test flow chart

of corrosion products, before and after TS. The morphology of these products was examined by using a JSM-6290 scanning electron microscope.

3 Results

3.1 TS + corrosion

Fig.3 shows the fatigue life resulting from various durations of thermal shock followed by 90 h of corrosion. As the figure shows, a low fatigue life is obtained in all cases. Corrosion may results in significant damage to AA7B04 and pitting on the specimen surface. The pits on the surface may act as fatigue sources, and thereby lead to shortening of the fatigue life. A comparison of the no TS and TS specimens reveals that the fatigue life of the former was 12%-15% shorter than that of the latter. The fatigue life of the TS specimens varied only slightly with increasing treatment time. Therefore, the TS process has a significant effect on the mechanical properties and fatigue life of AA7B04; The TS time has negligible influence, however, on these properties.

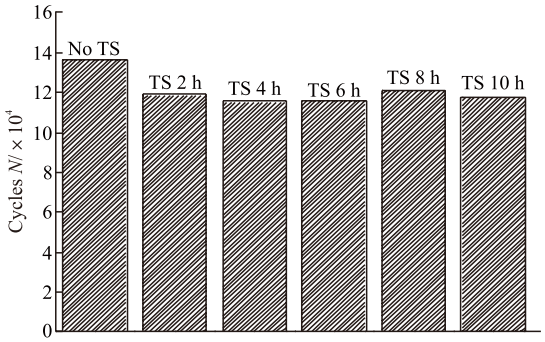

Fig.3 Fatigue life after "thermal shock for different time + corrosion"

Fig.4 shows the morphologies resulting from fatigue fracture. The corrosion pits on the specimen surface act as fatigue-crack initiation sites. The crack-initiation life was shortened owing to these pits, and hence crack generation was facilitated. As such, the fatigue life deceased after corrosion.

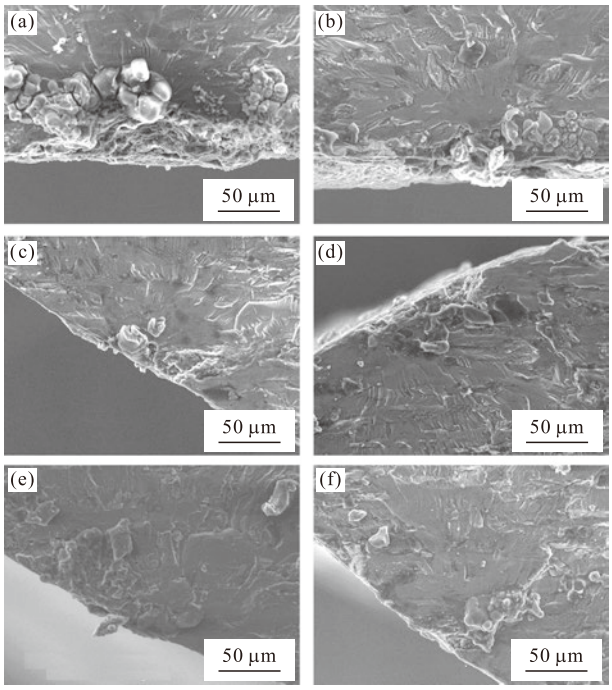

Fig.4 Fatigue fracture after "different time thermal shock+ corrosion": (a) no thermal shock; (b) thermal shock 2 h; (c) thermal shock 4 h; (d) thermal shock 6 h; (e) thermal shock 8 h; (f) thermal shock 10 h

3.2 Corrosion + TS + corrosion

Fig.5 shows the fatigue life resulting from 90 h of corrosion, TS for various times, and corrosion for another 90 h. The specimens all have low fatigue lives. A comparison of the TS specimens (no heat, TS 2 h, TS 6 h, TS 10 h) reveals that the fatigue life after 180 h of corrosion was shorter than that after 90 h of corrosion. The shortening of the fatigue life is attributed to prolonged corrosion. In fact, the fatigue life decreased with increasing corrosion time, albeit with differing levels of reduction. The fatigue life of the no TS specimen decreased more than that of the TS specimens. During both sets of tests, the fatigue life of the TS specimens decreased less than that of the no TS specimens after 180 h of corrosion at the same TS testing time. This indicates that the TS process has significant influence on the corrosion of AA7B04.

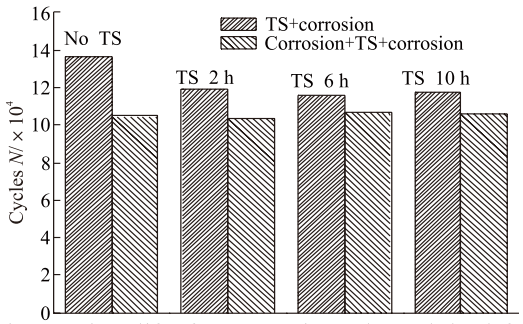

Fig.5 Fatigue life after "corrosion + thermal shock for different time + corrosion"

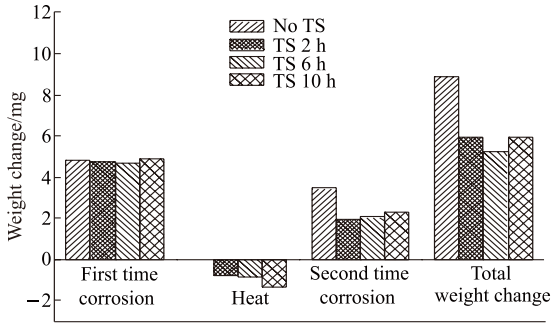

Fig.6 Specimens' weight changes at different states

Fig.6 shows the weight change of the specimens at different stages of testing. Positive and negative weight changes correspond to weight gain and weight loss, respectively. After the first round of corrosion, the weight of the specimens increased by almost the same amount. The weight of each specimen decreased after TS and the magnitude of the loss increased with increasing TS time. After the second round of corrosion, the weight of the specimens increased by varying degrees. The weight of the no TS specimens increased more than that of the TS specimens, which exhibited almost the same weight gain. Furthermore, a comparison of the total weight change reveals that the weight of the no TS specimens increased more than that of the TS specimens. This indicates that the no TS specimens were more severely corroded than their TS counterparts. In fact, the fatigue properties deteriorate with increasing severity of corrosion. The weight changes exhibit the same trends as those observed for the fatigue life (shown in Figs.3 and 5).

Fig. 7 shows the surface morphologies of the tested specimens. As the figure shows, corrosion products cover the surface of each specimen. A comparison of Fig.7 (a) and Fig.7 (c) reveals that the products on the no shock specimens were loose and porous. The AA7B04 matrix exhibited a poor corrosion resistance owing to this structure. After 10 h of TS, the products became smooth and dense and covered the surface completely, thereby resulting in excellent corrosion resistance of the AA7B04 matrix. A comparison of Fig.7 (b) and Fig.7 (d) reveals that the number and size (diameter) of the holes in the corrosion products of the no thermal shock specimen increased after second-time corrosion. Therefore, this specimen exhibits low corrosion resistance. Dense corrosion products, which are expected to prevent further corrosion of the AA7B04 matrix, formed on the 10 h TS specimen after second-time corrosion. As such, this specimen was less severely corroded, and hence its fatigue life decreased less than that of the no TS specimen.

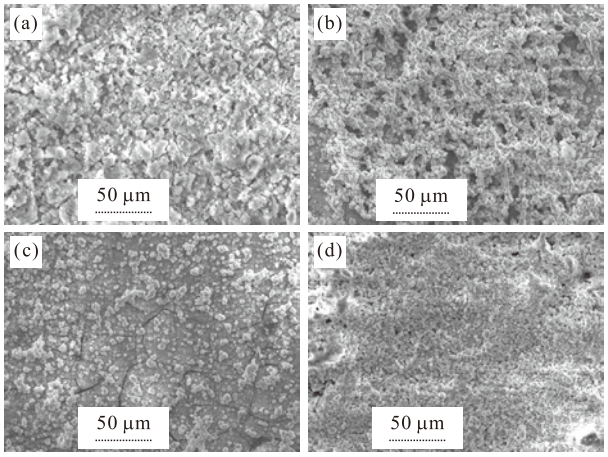

Fig.7 Surface morphologies: (a) after the first round of corrosion-no TS sample; (b) after the second round of corrosion-no TS sample; (c) after the first round of corrosion-10 h TS sample; (d) after the second round of corrosion-10 h TS sample

3.3 Corrosion + TS + corrosion + TS…+ corrosion

Fig. 8 shows the fatigue life after different cycles of corrosion and TS. As the figure shows, the fatigue life of the 10 cycles TS 10 h specimen is significantly higher than that of the one cycle TS 10 h specimen. In fact, for the same corrosion time (180 h), the fatigue life of the 10 cycles specimen was two times higher than that of the one cycle specimen. The results indicate that the fatigue life of corroded specimens subjected to repeated TS will decrease less than those subjected to a single cycle of TS.

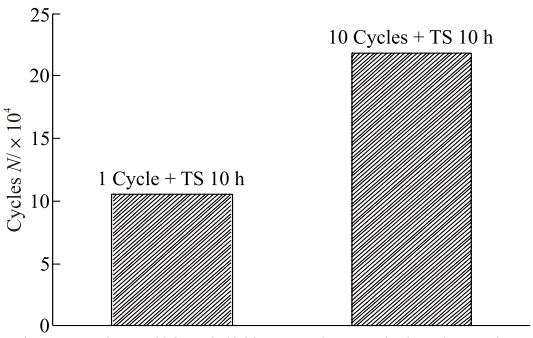

Fig.8 Fatigue life of different thermal shock cycles

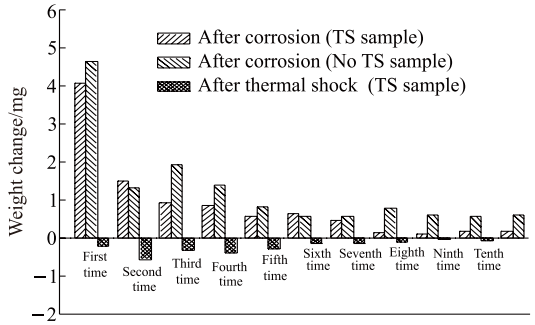

Fig.9 Specimens' weight changes at each cycles

Fig.9 shows the weight change of the specimens subjected to different testing conditions. As previously stated, positive and negative weight changes represent weight gain and weight loss, respectively. The weight changes, though significant in the first few loops, decreased with increasing number of cycles. In addition, the weight of the no TS specimen always increased, *i e*, the weight change decreased gradually during the first seven cycles and then remained approximately the same during the last three cycles. The weight change and overall weight of the TS specimen were lower than those of the no TS specimen. Moreover, the weight change decreased (in general) with increasing number of cycles for both increasing and decreasing weight of the TS specimens.

4 Discussion

The mechanical properties of the AA7B04 matrix and the degree of salt-spray corrosion may influence the fatigue life. The influence of the TS process on the fatigue life is manifested as: (a) a deterioration of the mechanical properties of the matrix and (b) changes in the structure and phase of the corrosion products.

4.1 Effect of the TS process on the mechanical properties

Table 1 Mechanical property changes after different time thermal shock

	UTS/MPa	YS/MPa	Final shrinkage/%
No thermal shock	537	596	32
Thermal shock 2 h	527	586	29
Thermal shock 4 h	520	578	28
Thermal shock 6 h	511	569	26
Thermal shock 8 h	505	560	23
Thermal shock 10 h	498	552	23

The ageing temperature of aluminum alloys is low and therefore artificial ageing occurred at 149 ℃. The mechanical properties of AA7B04 will change with varying TS time at 149 ℃. T6 was the peak ageing condition and hence the mechanical properties deteriorated (Table 1) with prolonged TS (*i e*, with the occurrence of artificial ageing).

4.2 Effect of the TS process on the corrosion products

Corrosion products were collected from the surface of the "no thermal shock + corrosion 180 h" specimens. Fig.10 (a) shows the TG and DSC curves of the products formed during TS at temperatures ranging from 40 to 250 ℃. As the figure shows, the weight of the products decreased at 150 ℃ (as indicated by the TG curve) and a small exothermic peak occurred in the DSC curve. The X-ray diffraction (XRD) patterns of the products before and after 1 h of TS are compared in Fig.10 (b). $Al(OH)_3$ was the main component in both cases, but the post-shock products also contained AlOOH, whose chemical formula (*i e*, $Al_2O_3 \cdot H_2O$) was determined by using the standard card. At room temperature and atmospheric pressure, $Al_2O_3 \cdot H_2O$ exhibits excellent corrosion resistance to a weak acidic solution and therefore serves as an excellent protective layer for AA7B04.

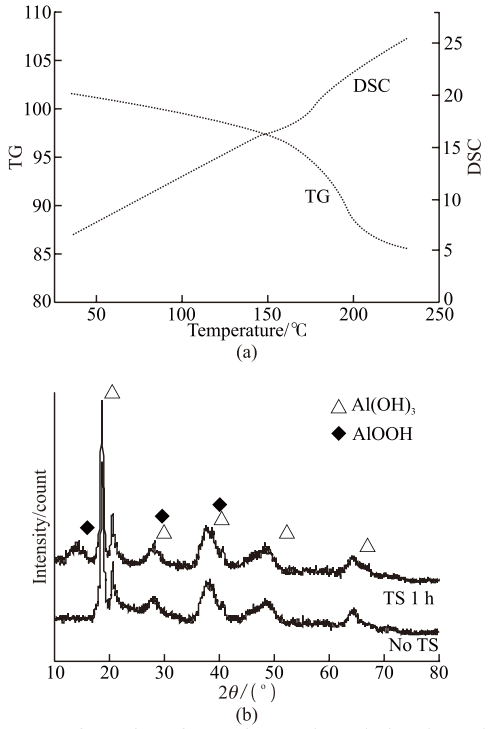

Fig.10 Transformation of corrosion products during thermal shock process: (a) TG and DSC curves; (b) XRD patterns of corrosion products before and after 1 h thermal shock

Fig.11 shows the XRD patterns of the specimens subjected to corrosion before and after TS for various times. Although absent from the pattern corresponding to the corrosion for 90 h no TS specimen (Fig.11 (a)), AlOOH peaks were present in patterns corresponding

to its thermal shock counterparts. This indicates that some of the $Al(OH)_3$ was transformed into AlOOH. A comparison of Figs.11 (a) and (b) reveals that AlOOH peaks persisted after a second-round of corrosion, indicating that AlOOH did not dissolve in the corrosion solution. Therefore, AlOOH exhibits excellent corrosion resistance and hence thermally shocked AA7B04 is less corroded than its no-TS counterpart. The reduction in the fatigue life decreased (shown in Figs.5 and.6) with decreasing amount of corrosion.

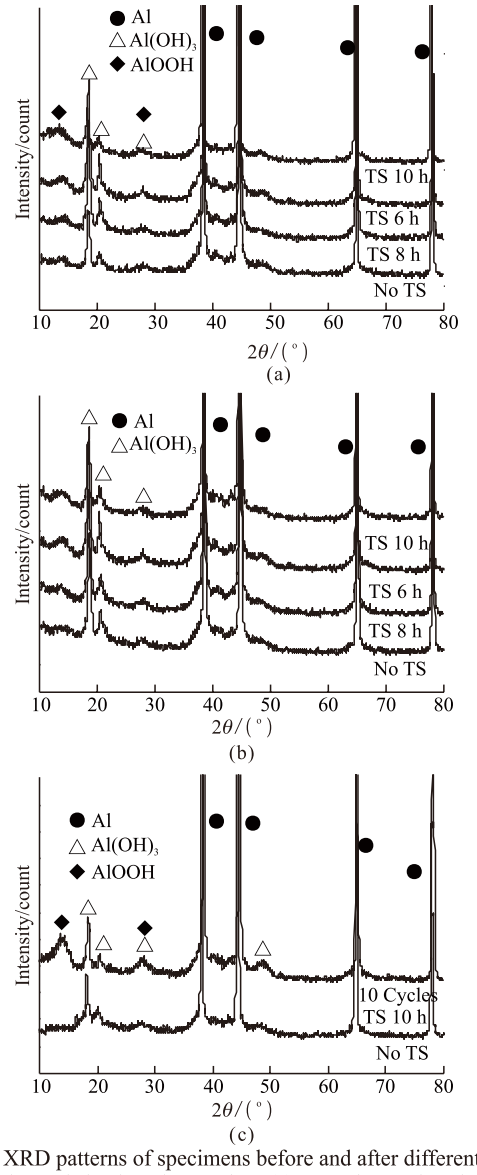

Fig.11 XRD patterns of specimens before and after different time thermal shock and corrosion: (a) corrosion 90 h + thermal shock for different time; (b) corrosion 90 h + thermal shock for different time + corrosion 90 h; (c) no thermal shock and 10 cycles thermal shock

Fig.11 (c) shows the XRD patterns of the no TS specimen and 10 cycle TS specimen. Peaks corresponding to AlOOH were absent from and present in the former and latter, respectively. The intensity of these peaks is higher than those of the single-cycle TS 10 h specimen (shown in Fig.11 (b)). Therefore, compared to that resulting from a single cycle, more $Al(OH)_3$ has been transformed into AlOOH and hence the corrosion resistance of AA7B04 is higher after several cycles of TS. As such, the fatigue life of the 10 cycle TS specimen was significantly higher than that of its single cycle counterpart.

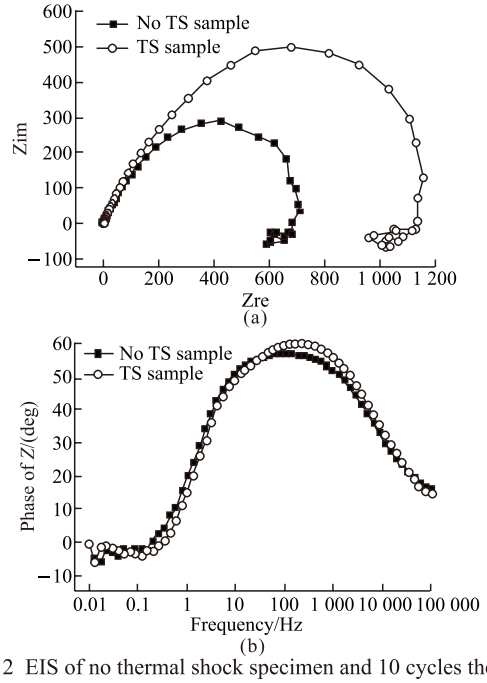

Fig.12 EIS of no thermal shock specimen and 10 cycles thermal shock 10 h specimen

Fig.12 shows the EIS plots corresponding to the no TS and 10 cycle TS samples. Both specimens were subjected to 180 h of corrosion, but exhibited different corrosion resistances. As Fig.12 (b) shows, two time constants occur in the Bode plots. In addition, the corresponding Nyquist plots consist of a capacitive reactance arc and an inductive reactance arc that occur in the high-frequency and low-frequency regions (Fig.12 (a)), respectively. The former represents the corrosion reaction of corrosion products on the AA7B04 in the solution; the latter corresponds to the pitting corrosion process of the matrix in a corrosive medium. Furthermore, the radius of the capacitive reactance arc corresponding to the 10 cycle TS specimen was significantly larger than that of the no TS specimen. The corrosion resistance of the 10 cycles TS specimen is therefore higher than that of the no TS specimen. This indicates that the TS process leads to improved corrosion resistance of the corrosion products. In the case of salt-mist corrosion, the 10 cycle TS specimen was less corroded, and hence had a

substantially higher post-corrosion fatigue life than its no TS counterpart (shown in Fig.8).

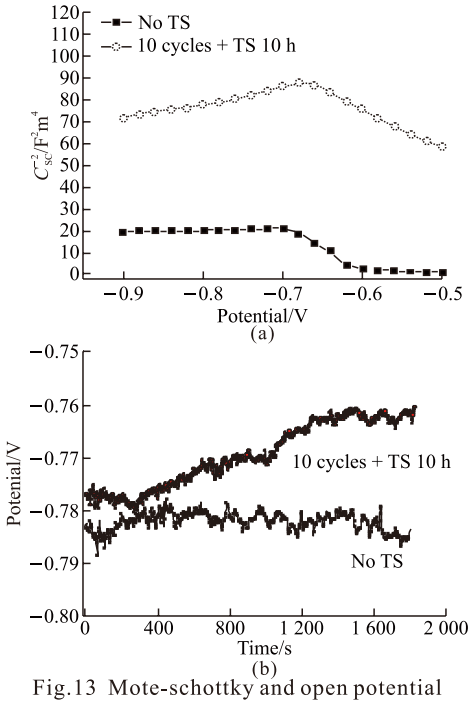

Fig.13 Mote-schottky and open potential

Table 2 Open potential and corresponding results

Potential range /V	Open potential /V	Specimen	k	N_D
−0.9--0.7	−0.785	No thermal shock	7.08	9.07×10^{28}
−0.9--0.7	−0.762	10 cycles thermal shock	67.52	9.51×10^{27}

Fig.13 shows the Mott-schottky curve and open potential of the no TS and 10 cycle TS 10 h specimens. These samples have open potential values of −0.762 (10 cycles TS) and −0.785 (no TS), as shown in Table 2. In addition, both curves had positive slopes (Fig.13 (a)), indicating that the corrosion products of these specimens are *n*-type semiconductors. For an *n*-type semiconductor: $\frac{1}{c^2} = \frac{2}{\varepsilon\varepsilon_0 e N_D}(E - E_{fb} - \frac{\kappa T}{e})$, where c, ε, ε_0, e, N_D, E_{fb}, k, and T are the space charge layer capacitance of the corrosion-product film, potential, actual permittivity (2.2 in this work), permittivity of vacuum, electron charge, electron donor concentration, flat-band potential, Boltzmann constant, and absolute

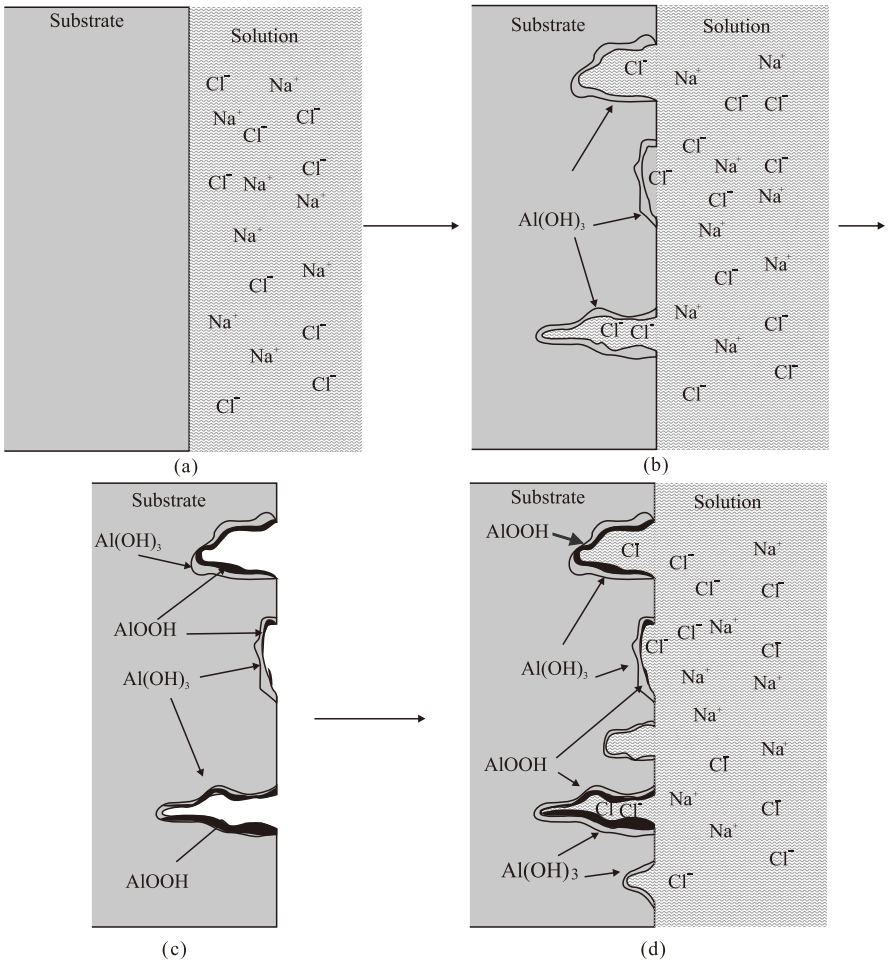

Fig.14 Transformation of pits and corrosion products during corrosion and thermal stock process

temperature, respectively; $\frac{2}{\varepsilon\varepsilon_0 e N_D}$ is the slop of curve k. N_D was determined by fitting the curve. The N_D value of the 10 cycle TS specimen is smaller than that of the no TS specimen. This indicates that the corrosion-product film of the 10 cycle specimen has a lower density of impurities than that of the no TS specimen; therefore, the 10 cycle specimen exhibits a higher resistance than its no TS counterpart. This results from the formation of dense AlOOH after TS, as indicated by the SEM and XRD results (shown in Fig.7 and Fig.11).

4.3 Transformation during corrosion and TS process

Fig.14 shows the transformation of the pits and corrosion products formed during the corrosion and TS process. The surface of the specimen was flat (process shown in Fig.14 (a)) at the beginning of the test. The passive films on the surface may become damaged, owing to Cl^- ions in the salt-mist atmosphere, and pitting corrosion occurs in some of the weak regions (see Fig.14(b)) during prolonged corrosion. Corrosion pits may act as fatigue crack initiation sites, thereby leading to a decrease in the fatigue life of the specimens. During the TS process, $Al(OH)_3$ may transform into AlOOH (process shown in Fig.14 (c)) owing to the effect of temperature. AlOOH exhibited excellent corrosion resistance to a weak acid solution and served as a protective layer for the AA7B04 matrix. Furthermore, the degree of corrosion decreased (process shown in Fig.14 (d)) when the specimens were subjected to a second round of corrosion. However, $Al(OH)_3$ may dissolve in the acid solution, thereby leading to a decrease in the acidity of the pit interior. The occluded-cell effect in the pits and pitting corrosion also decreased. Therefore, the pits formed during repeated corrosion/TS were all small and the fatigue life decreased only slightly after this process.

5 Conclusions

a) Thermal shocked at 149 ℃, AA7B04 would be subjected to aging process. This aging process may adversely affect the mechanical properties of the alloy. In fact, the mechanical properties of the alloy deteriorated with prolonged TS. After corrosion, the TS specimens had shorter fatigue lives than the no TS specimens.

b) TS at 149 ℃ may influence the composition and structure of the corrosion products. After TS, the products on the surface were denser (than those on the no TS specimens) and some of the $Al(OH)_3$ transformed into AlOOH. AlOOH exhibited better corrosion resistance than $Al(OH)_3$, and hence the denser AlOOH resulted in less severe corrosion. After corrosion, the fatigue life of the TS specimens decreased less than that of the no TS specimens.

c) The repeated corrosion/TS process may retard corrosion and result in only a slight decrease in the fatigue life. This observation differed from what happened under actual aircraft conditions. In other words, use of a continuous high-temperature TS to simulate a series of low-temperature TS processes would result in a large deviation between the test results and the actual situation. This, in turn, would adversely affect the life prediction of aircraft and influence flight safety.

References

[1] Jiang Z G, Tian D S, Zhou Z T. *Load/environment Spectrum of Aircraft Structure*[M]. Beijing: Electronic Industry Press, 2012

[2] Liu W T, Li Y H. *Evaluation Technique for Calendar Life System of Aircraft Structure*[M]. Beijing: Aviation Industry Press, 2004

[3] Dan Zhenhua, Muto Izumi, Hara Nobuyoshi. Effects of Environmental Factors on Atmospheric Corrosion of Aluminium and Its Alloys under Constant Dew Point Conditions[J]. *Corrosion Science*, 2012(57): 22-29

[4] Zupanca U, Grumb J. Effect of Pitting Corrosion on Fatigue Performance of Shot-peened Aluminium Alloy 7075-T651[J]. *Journal of Materials Processing Technology*, 2010, 210: 1 197-1 202

[5] Barter SA, Molent L. Fatigue Cracking from a Corrosion Pit in An Aircraft Bulkhead[J]. *Engineering Failure Analysis*, 2014, 39: 155-163

[6] Bao Rui, Zhang Xiang. Fatigue Crack Growth Behaviour and Life Prediction for 2324-T39 and 7050-T7451 Aluminium Alloys under Truncated Load Spectra[J]. *International Journal of Fatigue*, 2010, 32: 1 180-1 189

[7] Zheng Sanlong, Yu Qin, Gao Zengliang, *et al.* Loading History Effect on Fatigue Crack Growth of Extruded AZ31B Magnesium Alloy[J]. *Engineering Fracture Mechanics*, 2013, 114: 42-54

[8] Sunder R. Spectrum Load Fatigue-underlying Mechanisms and Their Significance in Testing and Analysis[J]. *International Journal of Fatigue*, 2003, 25: 971-981

[9] Chen Songyi, Chen Kanghua. Effect of Heat Treatment on Strength, Exfoliation Corrosion and Electrochemical Behavior of 7085 Aluminum Alloy [J]. *Materials and Design*, 2012, 35: 93-98

[10] Mohammad Azadi, Mehdi Mokhtari Shirazabadc. Heat Treatment Effect on Thermo-mechanical Fatigue and Low Cycle Fatigue Behaviors of A356.0 Aluminum Alloy[J]. *Materials and Design*, 2013, 45: 279-285

[11] Siddiqui RA, Abdul-Wahab SA, Pervez . Effect of Aging Time and Aging Temperature on Fatigue and Fracture Behavior of 6063 Aluminum Alloy under Seawater Influence[J]. *Materials and Design*, 2008, 29: 70-79

[12] Prasanta Kumar Rout, Ghosh MM, Ghosh KS. Effect of Interrupted Ageing on Stress Corrosion Cracking (SCC) Behaviour of An Al-Zn-Mg-Cu Alloy[J]. *Procedia Material Science*, 2014, 5: 1 214-1 223

[13] Mohammed Noor Desmukh, Pandey PK, Mukhopadhyay AK. Effect of Aging Treatments on the Kinetics of Fatigue Crack Growth in 7010 Aluminum Alloy[J]. *Materials Science and Engineering A*, 2006: 318-326

[14] Mitsuhiro Okayasun, Shoka Go. Precise Analysis of Effects of Aging on Mechanical Properties of Cast ADC12 Aluminum Alloy[J]. *Materials Science and Engineering A*, 2015, 638: 208-218

[15] Liu Yanjie, Wang Zhenyao, Ke Wei. Study on Influence of Native Oxide and Corrosion Products on Atmospheric Corrosion of Pure Al [J]. *Corrosion Science*, 2014, 80: 169-176

[16] Wang Xuehui, Wang Jihui, Fu Congwei. Characterization of Pitting Corrosion of 7A60 Aluminum Alloy by EN and EIS Techniques [J]. *Transactions of Nonferrous Metals Society of China*, 2014, 24: 3 907-3 916

[17] Liu Y, Meng GZ, Cheng YF. Electronic Structure and Pitting Behavior of 3003 Aluminum Alloy Passivated under Various Conditions[J]. *Electorchimica Acta*, 2009, 54: 4 155-4 160